

IXPE and NICER view of Black hole X-ray binary 4U 1630-47: First significant detection of polarized emission in thermal state

Ankur Kushwaha^{1,2*}, Kiran M. Jayasurya¹, Vivek K. Agrawal¹, Anuj Nandi¹

¹Space Astronomy Group, ISITE Campus, U. R. Rao Satellite Centre, Outer Ring Road, Marathahalli, Bangalore, 560037, India

²Department of Physics, Indian Institute of Science, Bangalore, 560012, India

Accepted XXX. Received YYY; in original form ZZZ

ABSTRACT

We present a detailed spectro-polarimetric study of Black hole X-ray binary 4U 1630 – 47 during its 2022 outburst with *IXPE* and *NICER* observations. The source is observed in disk dominated thermal state ($kT_{in} \approx 1.4$ keV) with clear detection of absorption features at 6.69 ± 0.01 keV and 6.97 ± 0.01 keV from both *NICER* as well as *IXPE* spectra, likely indicating a coupling of disk-wind. A significant degree of polarization (PD) = $8.33 \pm 0.17\%$ and polarization angle (PA) = $17.78^\circ \pm 0.60^\circ$ in the energy range of 2 – 8 keV are measured with *IXPE*. PD is found to be an increasing function of energy whereas PA remains roughly same within the energy range. Simultaneous energy spectra from *NICER* in the range of 0.5 – 12 keV are modelled to study the spectral properties. Furthermore, the spin parameter of the black hole is estimated with spectro-polarimetric data as $a_* = 0.920 \pm 0.001$ (1σ) which is corroborated by *NICER* observations. Finally, we discuss the implications of our findings.

Key words: accretion, accretion disks – polarization – techniques: polarimetric – black hole physics – radiation: dynamics – X-ray: binaries – stars: individual (4U 1630 – 47)

1 INTRODUCTION

The spectro-polarimetric study of the emission from Black hole X-ray binaries (BH-XRBs) can reveal the geometry and dynamics of accretion processes. This emission can be of thermal and non-thermal origins. The Keplerian accretion disk (Shakura & Sunyaev 1973) is considered to produce multi-colour thermal X-ray emission whereas inverse-comptonisation by a ‘hot’ corona (Titarchuk 1994; Tanaka & Lewin 1995; Chakrabarti & Titarchuk 1995) of soft photons emanating from disc is believed to be responsible for higher energy non-thermal emission. These two types of emissions are the major components in the energy spectra, of which one component may dominate in a spectral state of BH-XRBs (Homan et al. 2001; Homan & Belloni 2005; Remillard & McClintock 2006; Nandi et al. 2012; Baby et al. 2020; Kushwaha et al. 2021, and references therein).

The X-ray emission during soft state is expected to be linearly polarized parallel to the disk plane as the thermal emission suffers electron scattering in the inner disc region. Similarly, the emission in hard state is believed to be polarized as well but in the direction of normal to the disk plane. Since the seed photons from the disk are up-scattered within corona and produce polarized high energy photons (Stark & Connors 1977; Connors et al. 1980; Schnittman & Krolik 2009).

Apart from different spectral states, BH-XRBs are also known for their transient nature wherein the source exhibits sudden increase in flux after a prolonged quiescence phase (Lewin & Livingston 1995; Bildsten et al. 1997). Such outbursts can last from weeks to months

before the source fades into quiescence. The frequency and duration of these outbursts varies from source to source, or sometimes even among different outbursts of the same source itself (Homan et al. 2001; Belloni et al. 2005; Nandi et al. 2012; Sreehari et al. 2018, 2019, and references therein).

4U 1630 – 47 is a recurrent X-ray transient classified as a black hole candidate from its spectral and timing properties (Barret et al. 1996; Abe et al. 2005). It undergoes quasi-periodic outbursts with a recurrence time of ~ 600 days (Parmar et al. 1995). It is located near Galactic plane and has a high absorption column density with $N_H \sim 8 \times 10^{22} \text{ cm}^{-2}$ (Smith et al. 2002; Ueda et al. 2010) which makes it difficult to estimate the mass (M_{BH}), distance (D) and inclination (i) of the system. The best estimation of these parameters are $M_{BH} \sim 10 M_\odot$, $D = 10 \pm 0.1$ kpc and $i = 60^\circ - 70^\circ$ (Kuulkers et al. 1998; Tomsick et al. 1998; Augusteijn et al. 2001; Seifina et al. 2014). *NuSTAR* observations suggest that the source hosts a maximally rotating BH with spin parameter: $a_* = 0.985^{+0.005}_{-0.014}$ (King et al. 2014). Pahari et al. (2018) obtained the same as $0.92^{+0.02}_{-0.01}$ using *Chandra* and *AstroSat* observations of soft state during the 2016 outburst.

4U 1630 – 47, till date, has undergone more than 25 outbursts in the ~ 50 years since its detection in 1969. At the time of writing this letter, the source is found to be in another outburst. Moreover, polarization measurement during an outburst of 4U 1630 – 47, to the best of our knowledge, has not been reported so far.

In this work, we focus on the spectro-polarimetric study of 4U 1630 – 47 during its outburst which started on 28 July, 2022 and peaked on 21 August, 2022 (Jiang et al. 2022). Subsequent to an alert generated by *MAXI* (Mihara et al. 2011), *NICER* (Gendreau et al. 2016) and *IXPE* (Weisskopf et al. 2022) carried out long observations during the outburst under the target of opportunity (ToO) cam-

* E-mail: ankurksh@urc.gov.in

Table 1. Log of *NICER* and *IXPE* observations of 4U1630-47 considered in the analysis. From left to right, (1) name of observation; (2) observation ID; (3) start MJD of observation; (4) exposure time (5) unabsorbed flux, in units of $\times 10^{-9}$ ergs cm^{-2} s^{-1} in the mentioned energy range.

Obs Name	ObsID	Start MJD	Exposure (ksec)	Flux
NICER				
				0.5 – 10 keV
N1	5130010101	59790	~2.1	5.67
N2	5130010105	59799	~3.8	6.75
N3	5130010110	59805	~3.5	8.93
N4	5501010102	59814	~2.0	9.65
N5	5501010103	59815	~0.5	9.38
N6	5501010104	59816	~4.0	9.08
N7	5501010105	59817	~2.4	9.32
N8	5501010106	59818	~2.5	9.06
N9	5501010107	59819	~2.4	9.16
N10	5501010108	59820	~3.0	8.97
N11	5501010109	59821	~0.9	9.45
N12	5501010110	59822	~3.9	9.60
N13	5501010111	59823	~2.6	9.18
IXPE				
				1 – 10 keV
X1	01250401	59814	~460	4.03

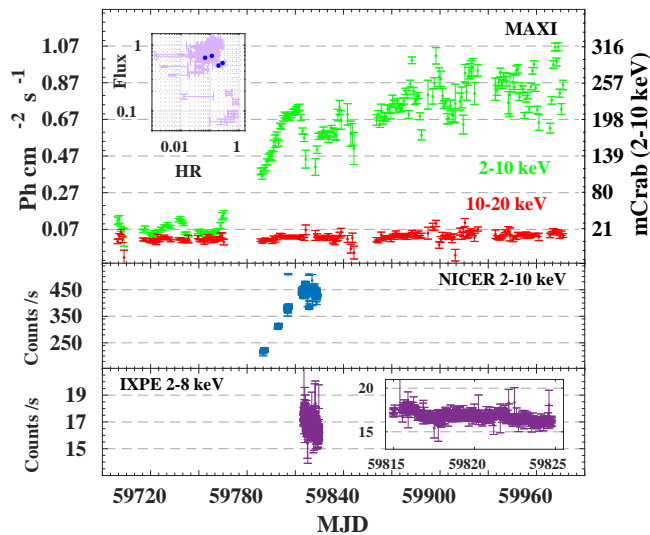


Figure 1. Top to bottom: 4U 1630 – 47 light curves obtained from *MAXI* (red and green), *NICER* (blue) and all three DUs of *IXPE* (purple). The inset in the top panel shows the HID from *MAXI* with blue dots corresponding to *IXPE* observation duration.

paign. We make use of *IXPE* and *NICER* data to study simultaneous polarimetric and spectral properties of 4U 1630 – 47 in 2 – 8 keV and 0.5 – 12 keV energy bands, respectively.

In §2, we provide details of the observations and the steps for data reduction. The outburst profile along with spectro-polarimetric data modelling using both *NICER* as well as *IXPE* are presented in §3. Finally, we discuss the results and conclude in §4.

2 OBSERVATIONS AND DATA REDUCTION

2.1 IXPE

IXPE is an imaging polarimeter (Weisskopf et al. 2022) consisting of three detector units (DUs) which are polarization sensitive in the 2 – 8 keV energy range. It observed 4U 1630 – 47 from 23 Aug, 2022

(MJD 59814) to 02 Sep, 2022 (MJD 59824) for ~460 ksec (Table 1). The Level-2 data of the observation are reduced and analysed with *IXPEOBSSIMv30.0.0* (Baldini et al. 2022) following the procedure of Farinelli et al. (2023). Further, *XPSELECT* task is used to extract the source and background event lists. The source is considered within a circular region of 60'' and the background region as an annular region with inner & outer radii of 180'' & 240'', respectively. Subsequently, the *XPBIN* task is used to generate the polarization cubes using the *PCUBE* algorithm. The Stokes I, Q and U spectra of source and background are generated with the *PHA1*, *PHA1Q* and *PHA1U* algorithms. The light curves in 2 – 8 keV energy band for the different DUs are generated with the *XSELECT* task of *HEASOFT v6.31.1* and added using the *lcmath* task to get a combined light curve (see bottom panel of Figure 1).

2.2 NICER

NICER observed the source from 30 Jul, 2022 (MJD 59790) to 01 Sep, 2022 (MJD 59823) which is well overlaps with *IXPE* observations (see Table 1 and Figure 1). Thirteen observations during this interval are analyzed covering the rising phase of the outburst as well as the peak of the same. The *NICERDASv10* software distributed with *HEASOFT v6.31.1* is used along with the latest *CALDB* to reduce the data from the observations. The *nicer12* task is used to perform standard calibration and screening to generate cleaned event lists. The source and background spectra along with the responses are generated in the 0.5 – 12 keV energy band using the *nicer13-spect* task. The spectra are rebinned to have a minimum of 25 counts per energy bin for spectral modelling. Further, the light curves for each observation (Figure 1) in the 2 – 10 keV energy range are generated using the *XSELECT* task.

3 MODELLING AND RESULTS

3.1 Light Curve and Outburst profile

We consider one day averaged *MAXI* light curves (see top panel of Figure 1) to get a comprehensive picture of the outburst of 4U 1630 – 47. The source, after ~150 days of inactivity goes into a new outburst in the last few days of July 2022. The *MAXI* count rate, in energy range of 2 – 10 keV, increases from its quiescent value of ~0.07 photons cm^{-2} s^{-1} to ~10 times on 21 August, 2022 (MJD 59812). At the time of writing this letter, the source is still in the outburst phase. Moreover, the hardness intensity diagram (HID) generated with *MAXI* flux (2 – 20 keV) and the hardness ratio (10 – 20 keV/2 – 10 keV) for the entire outburst duration represents an incomplete profile (see Figure 1) when compared with those of previous outbursts in 2016 and 2018 (Baby et al. 2020). It suggests that the source may remain in this phase for few more days before it declines to quiescent low hard state (LHS).

3.2 Spectral modelling

The variability observed in *MAXI* light curve of 4U 1630 – 47 motivates us to investigate spectral nature and its evolution during the outburst before we analyse the polarization measurement from *IXPE*. Therefore, we model *NICER* spectra, in 0.5 – 12 keV, of all the observations (see Table 1) starting from rising phase to peak of the outburst. We began with Obs. N1 and fit a phenomenological model: $\text{tbabs} * \text{diskbb}$. The residuals from the fit do not suggest any requirement of high energy power-law but an absorption below 4 keV

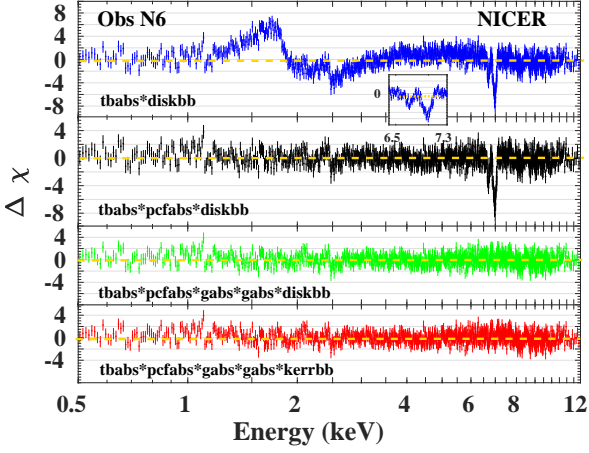


Figure 2. The residuals (in units of σ) for several models applied to the *NICER* spectra of 4U 1630 – 47 obtained from Obs. N6. The corresponding model is mentioned in each panel. The inset of top panel shows two absorption lines present at 6.69 keV and 6.97 keV.

is noticed (similar to top panel of Figure 2). Hence, a partial covering component *pcfabs* is multiplied in the model. This significantly improves the fit and results into a $\chi_{red}^2 = 1.10$. The instrument originated characteristic Gold emission lines from X-ray optics of *NICER* are corrected with inclusion of gauss components at 1.8 and 2.2 keV. Further, two additional line absorption features are clearly visible in the residual between 6 to 7 keV (similar to inset of Figure 2) and we model them with *gabs* components. These disk-wind originated absorption lines are reported previously and attributed to rest frame energies of Fe XXV and Fe XXVI lines at 6.697 keV and 6.966 keV, respectively (King et al. (2014); Pahari et al. (2018)). Finally, the overall fit results $\chi_{red}^2 = 1.02$ and a disk temperature of $kT_{in} = 1.12 \pm 0.01$ keV with absorption lines at energies 6.69 ± 0.01 keV and 6.97 ± 0.01 keV. The hydrogen column density N_H is estimated to be $(5.86 \pm 0.20) \times 10^{22}$ atoms cm^{-2} . The estimation of N_H is slightly lower than that of Pahari et al. (2018); Baby et al. (2020). This, we attribute to the presence of *pcfabs* in our model which also has N_H from covering column on top of interstellar medium column of hydrogen atoms. Further, similar fit procedure is applied to rest of the *NICER* observations from Obs. N2 to Obs. N13 with our final phenomenological non-relativistic model *tbabs*pcfabs*gabs*gabs*diskbb*. The residuals resulting at various steps of fit procedure and from models are provided in Figure 2 from Obs. N6 for illustration. The spectral fits indicate a disk dominated state of the source and a very stable disk temperature of $kT_{in} = 1.44 \pm 0.01$ keV is observed during peak of the outburst phase.

3.3 Spin estimation with Continuum Fitting (CF) method

The spectral modelling shows a disk dominated soft state of the source during outburst. In such state, the energy spectra are suitable for spin estimation with CF method. Hence, we make use of *NICER* spectra, observed later than the peak of the outburst (Obs. N4 to Obs. N13), to estimate the spin parameter of BH. We follow Kushwaha et al. (2021) to apply CF method and model the spectra with the relativistic model: *tbabs*pcfabs*gabs*gabs*kerrbb*. The model results into reasonably acceptable fits. The residuals, as previously, rule out any signature of power-law component in high energy till 12 keV (see bottom panel of Figure 2).

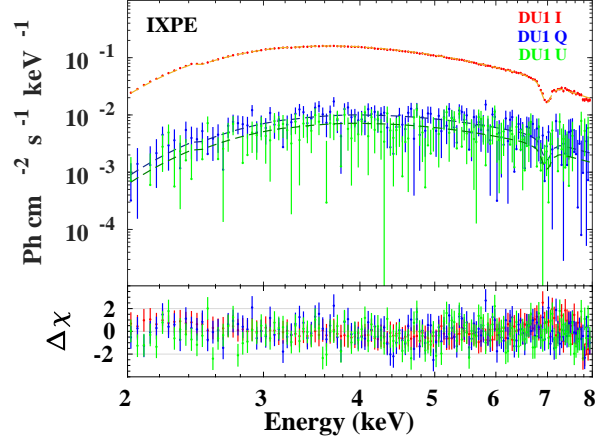


Figure 3. *IXPE* energy spectra (unfolded) of 4U 1630 – 47 during the outburst. Only DU1 Stokes I (red), Q (blue) and U (green) are shown along with fitted model (dashed line). Absorption feature at 6.9 keV is also present. The bottom panel shows the residuals in units of σ .

We switch off limb-darkening and apply zero torque condition at the inner boundary of the disk in *kerrbb* component. Moreover, the component is provided with the best estimations of distance to the source (D), inclination of the binary plane (i) and mass of the BH (M_{BH}) in the binary system based on the work of Pahari et al. (2018) and Baby et al. (2020). Therefore, we fix $D = 10$ kpc, $i = 65^\circ$, $M_{BH} = 10 M_\odot$. The spectral hardening factor (f) is fixed to a fiducial value of 1.55 (Shimura & Takahara 1995; Pahari et al. 2018). The other two parameters of *kerrbb* namely, accretion rate (\dot{M}) and spin parameter (a_*) are allowed to vary freely. For Obs. N4, the overall fit estimates $N_H = 6.38^{+0.19}_{-0.17} \times 10^{22}$ atoms cm^{-2} , $a_* = 0.933^{+0.002}_{-0.003}$ (1σ) and $\dot{M} = 1.62^{+0.04}_{-0.03} \times 10^{18}$ g s^{-1} with $\chi_{red}^2 = 0.99$ (898.05/908). Further, similar fit procedure is applied to rest of the observations to estimate the spin parameter. The residuals of best fit model are shown in Figure 2 from Obs. N6 for illustration. We notice that the relativistic model gives better fits (considering values χ_{red}^2) than the non-relativistic model and also results into consistent values of spin parameter from all the selected observations during the outburst of 4U 1630 – 47 along with model generated uncertainties. A detailed analysis with *NICER* data may be carried out for estimation and error analysis on spin parameter (see Kushwaha et al. 2021) which is out of scope of this work.

3.4 Polarimetric properties

IXPE observed ~ 460 ksec long portion of the outburst of 4U 1630 – 47. These observations spanned over ~ 10 days (see Table 1). Simultaneous observations by *NICER* reveal a stable spectral nature of system (see §3.2 & §3.3). Hence, *IXPE* observations are very suitable to study polarimetric properties for the first time from this source, using the methodology of Farinelli et al. (2023); Chatterjee et al. (2023); Jayasurya et al. (2023). Firstly, the model-independent PCUBE algorithm (Kislat et al. 2015) is used to determine the normalized Stokes parameters (Q/I & U/I), polarization angle (PA) and polarization degree (PD) in the 2 – 3.5 keV, 3.5 – 5 keV, 5 – 6.5 keV, 6.5 – 8 keV and in the total 2 – 8 keV energy ranges, during the Obs. X1. The normalized stokes parameter are provided in Table 3. PA and PD in four energy bands are given in Table 4 and corresponding plots with error contours are presented in Figure 4. We note that the source exhibits significant polarization,

Table 2. The best fit spectral parameters from *IXPE* observations of 4U1630-47 with relativistic model. From left to right are, (1) model components; (2) parameters in components; (3) best fit values for Obs. X1. The parameters that are fixed during the fits are denoted with ^{fixed}.

Components	Parameter	Value
<i>polpow</i>	A_{norm}	2.77 ± 0.32
	A_{index}	-0.76 ± 0.07
	psi_{norm}	17.72 ± 0.53
	$\text{psi}_{\text{index}}$	0^{fixed}
<i>tbabs</i>	N_{H}	5.84^{fixed}
<i>pcfabs</i>	N_{H}	4.78^{fixed}
<i>kerrbb</i>	CvrFract(%)	86.94^{fixed}
	a_*	0.920 ± 0.001
	\dot{M}	1.50 ± 0.01

with $\text{PD} = 8.33 \pm 0.17\%$ in 2 – 8 keV energy band with all the event data from three DUs combined. The PA in the same energy band is found to be $17.78^\circ \pm 0.60^\circ$. Moreover, we observe that PD has energy dependence whereas PA is roughly same over the energy range.

Subsequently, we also perform model-dependent analysis by fitting *IXPE* Stokes I, Q and U spectra in XSPEC. We borrow the relativistic model as described in §3.3 and insert the multiplicative component *polpow* which has PA and PD as function of energy. The component defines $\text{PD}(E) = A_{\text{norm}} \times E^{-A_{\text{index}}}$ and $\text{PA}(E) = \text{psi}_{\text{norm}} \times E^{-\text{psi}_{\text{index}}}$. The *polpow* is chosen over *polcont* component based on the results of PCUBE algorithm. Hence, the model *polpow*tbabs*gabs*gabs*pcfabs*kerrbb* is applied to fit three Stokes spectra from all the DUs of *IXPE* at once in XSPEC with the model. Only parameters of *polpow* component and a_* , \dot{M} of *kerrbb* are kept free for the fit. All other parameters are frozen to average values obtained from *NICER* spectral fits of Obs. N4 to Obs. N13. The fit results $\text{psi}_{\text{index}}$, as nearly zero and hence, it is fixed to zero which does not affect the overall fit. Finally, the fit procedure results into an acceptable $\chi_{\text{red}}^2 = 0.85$ for combined nine spectra (I, Q & U for 3 DUs). The best fit values are provided in the Table 2. The overall fit of the spectra is shown in Figure 3. Furthermore, the model-dependent polarization results are compared with those obtained in model-independent method by integrating $\text{PA}(E)$ and $\text{PD}(E)$ in the 2 – 8 keV energy band which results $\text{PA} \sim 17.72^\circ$ and $\text{PD} \sim 9\%$. We notice PA and PD from two different approaches of PCUBE and XSPEC are in good agreement. We outline that the spin parameters resulting from *NICER* spectral fits and *IXPE* polarimetric fits are also in good agreement.

4 DISCUSSION AND CONCLUSION

In this letter, we report the significant detection of X-ray polarization from a recurrent transient BH-XRB 4U 1630 – 47 by *IXPE* during its outburst in 2022. The polarization properties are consolidated with simultaneous spectral studies by *NICER* observations.

The most intriguing finding from our investigation is a substantial degree of polarization ($\text{PD} = 8.33 \pm 0.17\%$ ($> 48\sigma$ statistical confidence) in disk dominated outburst phase of the source in 2 – 8 keV energy range. The energy resolved PD reaches as high as $11.02 \pm 0.92\%$ ($> 11\sigma$ statistical confidence) in 6.5 – 8 keV. These measurements are significantly higher when compared to those predicted from existing models (Dovčiak et al. 2008; Schnittman & Krolik 2009; Taverna et al. 2020). Although the increasing nature of PD within 2 – 8 keV energy range is similar as depicted by the models. This

Table 3. Normalized Stokes parameters (with 1σ errors), obtained from *IXPE* observation of 4U 1630 – 47 computed with the PCUBE algorithm in four different energy bins.

	DU1	DU2	DU3	All DUs
2 – 8 keV				
Q/I (%)	6.74 ± 0.29	6.47 ± 0.30	7.14 ± 0.30	6.78 ± 0.17
U/I (%)	4.23 ± 0.29	4.96 ± 0.30	5.38 ± 0.30	4.85 ± 0.17
2 – 3.5 keV				
Q/I (%)	5.63 ± 0.40	4.46 ± 0.41	5.81 ± 0.42	5.30 ± 0.24
U/I (%)	3.45 ± 0.40	4.27 ± 0.41	4.04 ± 0.42	3.91 ± 0.24
3.5 – 5 keV				
Q/I (%)	6.29 ± 0.38	6.72 ± 0.39	7.12 ± 0.39	6.70 ± 0.22
U/I (%)	3.89 ± 0.38	4.71 ± 0.39	5.61 ± 0.39	4.71 ± 0.22
5 – 6.5 keV				
Q/I (%)	8.23 ± 0.64	8.38 ± 0.66	7.49 ± 0.66	8.04 ± 0.38
U/I (%)	5.43 ± 0.64	6.75 ± 0.66	6.52 ± 0.66	6.22 ± 0.38
6.5 – 8 keV				
Q/I (%)	9.33 ± 1.55	8.09 ± 1.64	11.30 ± 1.61	9.57 ± 0.92
U/I (%)	5.74 ± 1.55	4.18 ± 1.64	6.49 ± 1.61	5.48 ± 0.92

Table 4. PD and PA (with 1σ errors), obtained from *IXPE* observation of 4U 1630 – 47 computed with the PCUBE algorithm in different energy bins

	2 – 8 keV	2 – 3.5 keV	3.5 – 5 keV	5 – 6.5 keV	6.5 – 8 keV
PCUBE					
PD (%)	8.33 ± 0.17	6.58 ± 0.24	8.19 ± 0.22	10.17 ± 0.38	11.02 ± 0.92
PA (°)	17.78 ± 0.60	18.21 ± 1.02	17.56 ± 0.78	18.87 ± 1.06	14.90 ± 2.40

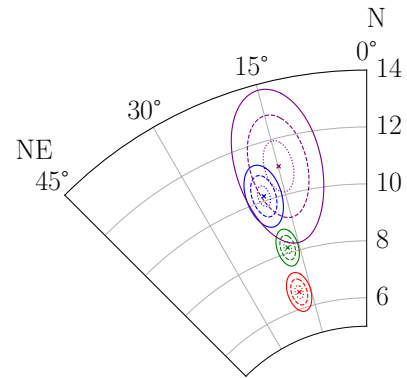


Figure 4. The confidence contours (1σ [dotted], 2σ [dashed] and 3σ [solid]) of PA and PD obtained with *IXPE* in 2 – 3.5 (red), 3.5 – 5 (green), 5 – 6.5 (blue) and 6.5 – 8 keV (purple) energy bins. The grid shows PA (°) on radial lines and PD (%) as concentric rings.

indicates that additional physical processes and effects are in play on top of electron scattering on the surface of disk along with reflection of return radiation from the near side of the disk which can further enhance the PD.

Recently, Krawczynski et al. (2022) reported polarization properties of Cygnus X-1 in LHS, and found that the observed PD is approximately twice as high as expected. These polarimetric results favour the presence of the coronal plasma in wedge shaped geometry within the system. In the case of 4U 1630 – 47, such strong Compton scattering medium like corona may not be present as the *NICER*

spectra during the outburst show no signature of high energy tail. But, a weak corona may be present as observed in previous outbursts (Pahari et al. 2018; Baby et al. 2020). A weak corona may contribute to some extent in the net observed PD.

Another plausible contribution in PD could be from scattering of the photons in an obscuring medium generated by disk-wind between inner regions of the disk and an observer. The strong evidence of disk-wind comes from the *NICER* spectral modelling. The spectra during the outburst exhibit presence of partial covering over the disk radiation and absorption line features of Fe XXV and Fe XXVI at rest frame energies 6.697 keV and 6.966 keV respectively (see Figure 2). These absorption features are also present in *IXPE-I* spectrum but the two lines are merged, resulting in a broad absorption dip (see Figure 3). Due to poor statistics, the presence of the absorption feature is not clear in *IXPE-Q* and *U* spectra. Although the difference in intensities of the absorption lines, if they were present, in *Q* and *U* spectra would have provided an important piece of evidence about the origin of polarized emission from disk-wind. Recently, similar absorption features associated with disk-wind are also observed in outburst of 4U 1543 – 47 (Prabhakar et al. 2023).

Disk-wind in soft states may have a column density up to $N_H \sim 10^{25} \text{ cm}^{-2}$ in the equatorial direction. A rough qualitative estimates are provided and discussed by Ratheesh et al. (2021). The wind may be fully ionized but Compton thick in the equatorial direction. The effective column density and therefore PD may vary with inclination angle (i) with respect to a distant observer. Hence, the polarized signature of 4U 1630 – 47 may be affected by disk-wind and its geometry.

We also estimate the associated electric field angle as $PA = 17.78^\circ \pm 0.60^\circ$ which remains mostly same within the 2 – 8 keV energy range of *IXPE*. The paucity of radio observations and measurements of jet angle from the source prevented us to relate it with geometry of the system. Although we note that the PA is comparable to 90° minus the inclination of the binary plane. In case of Cygnus X-1, PA is found to align with jet angle, which is assumed to be parallel to BH spin axis or normal to disk plane (Krawczynski et al. 2022).

Furthermore, PD and PA are estimated with spectro-polarimetric modelling in XSPEC as $\sim 9\%$ and $\sim 17.72^\circ$, respectively. These model-dependent estimations of PD and PA are in good agreement with those computed from model-independent *PCUBE* algorithm. The values lie within 3σ uncertainties.

The spectro-polarimetric fit of *IXPE* data with relativistic model also constrains the BH spin parameter: $a_* = 0.920 \pm 0.001$ (1σ) and accretion rate: $\dot{M} = (1.50 \pm 0.01) \times 10^{18} \text{ g s}^{-1}$. The \dot{M} is shown to be related to the mass loss rate through disk-wind outflow in 4U 1630 – 47 and other BH-XRBs (Neilsen et al. 2011; Ponti et al. 2012).

We compare the value of a_* with that obtained by applying CF method on *NICER* spectra during peak of the outburst which resulted $a_* = 0.933^{+0.002}_{-0.003}$ (1σ). The spin parameter estimated with two different approaches are in good agreement. The estimations are also in line with findings of Pahari et al. (2018), whereas King et al. (2014) indicated presence of a maximally rotating BH in the system. Recent measurement by *Insight-HXMT* suggests a slow rotating BH with $a_* = 0.817 \pm 0.014$ (90% statistical error) Liu et al. (2022). Here, we highlight the fact that estimation of spin parameter is highly dependent on i , D and M .

To summarize, we report a significant detection of polarized emission from 4U 1630 – 47 during its outburst in 2022. The observed high degree of polarization may be due to combined effects from the accretion disk, disk-wind and a weak corona in the system. The spin

of the black hole is also estimated with spectro-polarimetric data of *IXPE*.

ACKNOWLEDGEMENTS

We thank the anonymous reviewer for careful reading of our manuscript to provide insightful comments and suggestions that significantly improved the manuscript in terms of both science as well as writing. Authors thank GH, SAG; DD, PDMSA and Director, URSC for encouragement and continuous support to carry out this research. *IXPE*, *NICER* and *MAXI* teams are also thanked for providing data products and software tools for data analysis.

DATA AVAILABILITY

Data used for this work are available at *HEASARC* website (<https://heasarc.gsfc.nasa.gov/docs/archive.html>) and *MAXI* website (<http://maxi.riken.jp/top/index.html>).

REFERENCES

- Abe Y., Fukazawa Y., Kubota A., Kasama D., Makishima K., 2005, *PASJ*, **57**, 629
- Augusteijn T., Kuulkers E., van Kerkwijk M. H., 2001, *A&A*, **375**, 447
- Baby B. E., Agrawal V. K., Ramadevi M. C., Katoch T., Antia H. M., Mandal S., Nandi A., 2020, *MNRAS*, **497**, 1197
- Baldini L., et al., 2022, *SoftwareX*, **19**, 101194
- Barret D., McClintock J. E., Grindlay J. E., 1996, *ApJ*, **473**, 963
- Belloni T., Homan J., Casella P., van der Klis M., Nespoli E., Lewin W. H. G., Miller J. M., Méndez M., 2005, *A&A*, **440**, 207
- Bildsten L., et al., 1997, *ApJS*, **113**, 367
- Chakrabarti S., Titarchuk L. G., 1995, *ApJ*, **455**, 623
- Chatterjee R., Agrawal V. K., Jayasurya K. M., Katoch T., 2023, *arXiv e-prints*, p. arXiv:2301.13394
- Connors P. A., Piran T., Stark R. F., 1980, *ApJ*, **235**, 224
- Dovčiak M., Muleri F., Goosmann R. W., Karas V., Matt G., 2008, *MNRAS*, **391**, 32
- Farinelli R., et al., 2023, *MNRAS*, **519**, 3681
- Gendreau K. C., et al., 2016, in den Herder J.-W. A., Takahashi T., Bautz M., eds, Society of Photo-Optical Instrumentation Engineers (SPIE) Conference Series Vol. 9905, Space Telescopes and Instrumentation 2016: Ultraviolet to Gamma Ray. p. 99051H, doi:10.1117/12.2231304
- Homan J., Belloni T., 2005, *Ap&SS*, **300**, 107
- Homan J., Wijnands R., van der Klis M., Belloni T., van Paradijs J., Klein-Wolt M., Fender R., Méndez M., 2001, *ApJS*, **132**, 377
- Jayasurya K. M., Agrawal V. K., Chatterjee R., 2023, *arXiv e-prints*, p. arXiv:2302.03396
- Jiang J., Tomsick J., Liu H., Fabian A., Connors R., Garcia J., Hare J., 2022, *The Astronomer's Telegram*, **15575**, 1
- King A. L., et al., 2014, *ApJ*, **784**, L2
- Kislat F., Clark B., Beilicke M., Krawczynski H., 2015, *Astroparticle Physics*, **68**, 45
- Krawczynski H., et al., 2022, *Science*, **378**, 650
- Kushwaha A., Agrawal V. K., Nandi A., 2021, *MNRAS*, **507**, 2602
- Kuulkers E., Wijnands R., Belloni T., Méndez M., van der Klis M., van Paradijs J., 1998, *ApJ*, **494**, 753
- Lewin W. H. G., Livingston W., 1995, *Journal of the British Astronomical Association*, **105**, 284
- Liu Q., Liu H., Bambi C., Ji L., 2022, *MNRAS*, **512**, 2082
- Mihara T., et al., 2011, *PASJ*, **63**, S623
- Nandi A., Debnath D., Mandal S., Chakrabarti S. K., 2012, *A&A*, **542**, A56
- Neilsen J., Remillard R. A., Lee J. C., 2011, *ApJ*, **737**, 69
- Pahari M., et al., 2018, *ApJ*, **867**, 86

- Parmar A. N., Angelini L., White N. E., 1995, [ApJ](#), **452**, L129
- Ponti G., Fender R. P., Begelman M. C., Dunn R. J. H., Neilsen J., Coriat M., 2012, [MNRAS](#), **422**, L11
- Prabhakar G., Mandal S., G R B., Nandi A., 2023, [MNRAS](#),
- Ratheesh A., Tombesi F., Fukumura K., Soffitta P., Costa E., Kazanas D., 2021, [A&A](#), **646**, A154
- Remillard R. A., McClintock J. E., 2006, [ARA&A](#), **44**, 49
- Schnittman J. D., Krolik J. H., 2009, [ApJ](#), **701**, 1175
- Seifina E., Titarchuk L., Shaposhnikov N., 2014, [ApJ](#), **789**, 57
- Shakura N. I., Sunyaev R. A., 1973, [A&A](#), **500**, 33
- Shimura T., Takahara F., 1995, [ApJ](#), **445**, 780
- Smith R. K., Edgar R. J., Shafer R. A., 2002, [ApJ](#), **581**, 562
- Sreehari H., Nandi A., Radhika D., Iyer N., Mandal S., 2018, [Journal of Astrophysics and Astronomy](#), **39**, 5
- Sreehari H., Ravishankar B. T., Iyer N., Agrawal V. K., Katoch T. B., Mandal S., Nandi A., 2019, [MNRAS](#), **487**, 928
- Stark R. F., Connors P. A., 1977, [Nature](#), **266**, 429
- Tanaka Y., Lewin W. H. G., 1995, in X-ray Binaries. pp 126–174
- Taverna R., Zhang W., Dovčiak M., Bianchi S., Bursa M., Karas V., Matt G., 2020, [MNRAS](#), **493**, 4960
- Titarchuk L., 1994, [ApJ](#), **434**, 570
- Tomsick J. A., Lapshov I., Kaaret P., 1998, [ApJ](#), **494**, 747
- Ueda Y., et al., 2010, [ApJ](#), **713**, 257
- Weisskopf M. C., et al., 2022, [Journal of Astronomical Telescopes, Instruments, and Systems](#), **8**, 026002

This paper has been typeset from a $\text{\TeX}/\text{\LaTeX}$ file prepared by the author.